Research Article | Vol. 7, No. 12 | 1 Dec 2017 | OPTICAL MATERIALS EXPRESS 4328
Optical Materials EXPRESS

Barium titanate ($BaTiO_3$) RF characterization for application in electro-optic modulators

ALVARO ROSA,[1] DOMENICO TULLI,[2] PAU CASTERA,[1] ANA M. GUTIERREZ,[1] AMADEU GRIOL,[1] MARIANO BAQUERO,[1] BERTRAND VILQUIN,[3] FELIX ELTES,[4] STEFAN ABEL,[4] JEAN FOMPEYRINE,[4] AND PABLO SANCHIS[1,*]

[1]*Nanophotonics Technology Center, Universitat Politècnica de València, Camino de Vera s/n, Valencia 46022, Spain*
[2]*DAS Photonics, S. L., Universitat Politecnica Valencia, Valencia 46022, Spain*
[3]*Institut des Nanotechnologies de Lyon, 69134 Ecully Cedex, Lyon, France*
[4]*IBM Research–Zurich, Säumerstrasse 4, CH-8803 Rüschlikon, Switzerland*
**pabsanki@ntc.upv.es*

Abstract: Barium titanate ($BaTiO_3$ or BTO) is currently one of the most promising ferroelectric materials for enabling Pockels modulation that is compatible with silicon photonic circuits. The relative permittivity of BTO has been characterized in thin films deposited on a silicon-on-insulator (SOI) substrate. High values between 800 and 1600 have been estimated at 20 GHz. Furthermore, no substantial difference has been obtained by using BTO grown by molecular beam epitaxy and sputtering. The obtained permittivity has been used to properly design the RF electrodes for high-speed modulation in hybrid BTO/Si devices. Electrodes have been fabricated and the possibility of achieving modulation bandwidths up to 40 GHz has been demonstrated. The bandwidth is limited by the microwave propagation losses and, in this case, different losses have been measured depending on the BTO growth process.

OCIS codes: (230.2090) Electro-optical devices; (250.5300) Photonic integrated circuits.

References and links

1. M. E. Lines and A. M. Glass, *Principles and Applications of Ferroelectrics and Related Materials* (Oxford University Press, 2001).
2. D. Hennings, "Barium titanate based ceramic materials for dielectric use," Int. J. High Technol. Ceram. **3**, 91–111 (1987).
3. L. Sengupta and S. Sengupta, "Novel ferroelectric materials for phased array antennas," IEEE Trans. Ultrason. Ferroelectr. Freq. Control **44**, 792–797 (1997).
4. F. De Flaviis, N. G. Alexopoulos, and O. M. Stafsudd, "Planar microwave integrated phase-shifter design with high purity ferroelectric material," IEEE Trans. Microw. Theory Tech. **45**, 963–969 (1997).
5. M. Zgonik, P. Bernasconi, M. Duelli, R. Schlesser, P. Günter, M. H. Garrett, D. Rytz, Y. Zhu, and X. Wu, "Dielectric, elastic, piezoelectric, electro-optic, and elasto-optic tensors of $BaTiO_3$ crystals," Phys. Rev. B Condens. Matter **50**(9), 5941–5949 (1994).
6. G. T. Reed, G. Mashanovich, F. Y. Gardes, and D. J. Thomson, "Silicon optical modulators," Nat. Photonics **4**, 518–526 (2010).
7. A. Petraru, J. Schubert, M. Schmid, and C. Buchal, "Ferroelectric $BaTiO_3$ thin-film optical waveguide modulators," Appl. Phys. Lett. **81**, 1375–1377 (2002).
8. P. Tang, D. Towner, T. Hamano, A. Meier, and B. Wessels, "Electrooptic modulation up to 40 GHz in a barium titanate thin film waveguide modulator," Opt. Express **12**(24), 5962–5967 (2004).
9. P. Tang, A. L. Meier, D. J. Towner, and B. W. Wessels, "BaTiO3 thin-film waveguide modulator with a low voltage-length product at near-infrared wavelengths of 0.98 and 1.55 μm," Opt. Lett. **30**(3), 254–256 (2005).
10. M. J. Dicken, L. A. Sweatlock, D. Pacifici, H. J. Lezec, K. Bhattacharya, and H. A. Atwater, "Electrooptic modulation in thin film barium titanate plasmonic interferometers," Nano Lett. **8**(11), 4048–4052 (2008).
11. P. Girouard, Z. Liu, P. Chen, Y. K. Jeong, Y. Tu, S.-T. Ho, and B. W. Wessels, "Enhancement of the pockels effect in photonic crystal modulators through slow light," Opt. Lett. **41**(23), 5531–5534 (2016).
12. S. Abel, T. Stöferle, C. Marchiori, C. Rossel, M. D. Rossell, R. Erni, D. Caimi, M. Sousa, A. Chelnokov, B. J. Offrein, and J. Fompeyrine, "A strong electro-optically active lead-free ferroelectric integrated on silicon," Nat. Commun. **4**, 1671 (2013).

#302285 https://doi.org/10.1364/OME.7.004328
Journal © 2017 Received 13 Jul 2017; revised 18 Sep 2017; accepted 8 Oct 2017; published 10 Nov 2017

Optical Materials EXPRESS

13. C. Xiong, W. H. P. Pernice, J. H. Ngai, J. W. Reiner, D. Kumah, F. J. Walker, C. H. Ahn, and H. X. Tang, "Active silicon integrated nanophotonics: ferroelectric $BaTiO_3$ devices," Nano Lett. **14**(3), 1419–1425 (2014).
14. S. Abel, T. Stöferle, C. Marchiori, D. Caimi, L. Czornomaz, M. Stuckelberger, M. Sousa, B. J. Offrein, and J. Fompeyrine, "A hybrid barium titanate-silicon photonics platform for ultra efficient electro-optic tuning," J. Lightwave Technol. **34**, 1688–1693 (2016).
15. F. Eltes, D. Caimi, F. Fallegger, M. Sousa, E. O'Connor, M. D. Rossell, B. Offrein, J. Fompeyrine, and S. Abel, "Low-Loss $BaTiO_3$-Si Waveguides for Nonlinear Integrated Photonics," ACS Photonics **3**, 1698–1703 (2016).
16. M.-H. M. Hsu, A. Marinelli, C. Merckling, M. Pantouvaki, J. Van Campenhout, P. Absil, and D. Van Thourhout, "Orientation-dependent electro-optical response of $BaTiO_3$ on $SrTiO_3$-buffered Si(001) studied via spectroscopic ellipsometry," Opt. Mater. Express **7**, 2030 (2017).
17. P. Rabiei, J. Ma, S. Khan, J. Chiles, and S. Fathpour, "Heterogeneous lithium niobate photonics on silicon substrates," Opt. Express **21**(21), 25573–25581 (2013).
18. W. H. P. Pernice, C. Xiong, F. J. Walker, and H. X. Tang, "Design of a silicon integrated electro-optic modulator using ferroelectric $BaTiO_3$ Films," IEEE Photonics Technol. Lett. **26**, 1344–1347 (2014).
19. X. Hu, S. Cueff, P. R. Romeo, and R. Orobtchouk, "Modeling the anisotropic electro-optic interaction in hybrid silicon-ferroelectric optical modulator," Opt. Express **23**(2), 1699–1714 (2015).
20. P. Castera, D. Tulli, A. M. Gutierrez, and P. Sanchis, "Influence of $BaTiO_3$ ferroelectric orientation for electro-optic modulation on silicon," Opt. Express **23**(12), 15332–15342 (2015).
21. P. Castera, A. M. Gutierrez, D. Tulli, S. Cueff, R. Orobtchouk, P. R. Romeo, G. Saint-Girons, and P. Sanchis, "Electro-Optical Modulation Based on Pockels Effect in $BaTiO_3$ with a Multi-Domain Structure," IEEE Photonics Technol. Lett. **28**, 990–993 (2016).
22. C. A. T. Siciunas and E. Salama, "Characteristics of RF Sputtered Barium Titanate Films on Silicon," J. Vac. Sci. Technol. **9**, 91 (1972).
23. T. Hayashi, N. Oji, and H. Maiwa, "Film thickness dependence of dielectric properties of $BaTiO_3$ thin films prepared by sol-gel method," Jpn. J. Appl. Phys. **33**, 5277–5280 (1994).
24. T. Hamano, D. J. Towner, and B. W. Wessels, "Relative dielectric constant of epitaxial $BaTiO_3$ thin films in the GHz frequency range," Appl. Phys. Lett. **83**, 5274–5276 (2003).
25. R. A. McKee, F. J. Walker, J. R. Conner, E. D. Specht, and D. E. Zelmon, "Molecular beam epitaxy growth of epitaxial barium silicide, barium oxide, and barium titanate on silicon," Appl. Phys. Lett. **59**, 782–784 (1991).
26. K. Schraml and D. Heberling, "Estimation of the propagation constant in multilayer microwave circuits using a low cost multiline system," in 2015 Loughborough Antennas and Propagation Conference, LAPC **2015**, 1–4 (2015).
27. M. D. Janezic and J. a. Jargon, "Complex permittivity determination from propagation constant measurements," IEEE Microw. Guided Wave Lett. **9**, 76–78 (1999).
28. G. F. Engen and C. A. Hoer, "Thru-Reflect-Line: An Improved Technique for Calibrating the Dual Six-Port Automatic Network Analyzer," IEEE Trans. Microw. Theory Tech. **27**, 987–993 (1979).
29. K. Wu and L. Li, "Numerical calibration and de-embedding techniques for CAD and equivalent circuit models of electromagnetic structures," Microw. Rev. June, 7–19 (2005).
30. R. O. D. C. Alferness, "Waveguide Electrooptic Modulators," IEEE Trans. Microw. Theory Tech. **30**, 1121–1137 (1982).
31. D. M. Pozar, *Microwave engineering* (Addison-Wesley Publ. Co., 1993).
32. H. Chung, W. S. C. Chang, and E. L. Adler, "Modeling and Optimization of Traveling-Wave $LiNbO_3$ Interferometric Modulators," IEEE J. Quantum Electron. **27**, 608–617 (1991).

1. Introduction

Ferroelectric materials with high permittivity have been largely investigated for ceramic applications [1, 2]. However, these materials have also found application in other fields such as phased array antennas [3] or planar microwave integrated phase shifter [4]. In this context, barium titanate ($BaTiO_3$ or BTO) is one of the most representative ferroelectric materials. For photonic applications, BTO is one of the best candidates to develop high performance electro-optical modulators thanks to its large Pockels coefficients [5]. The Pockels coefficients in bulk BTO crystals is several orders of magnitude higher than lithium niobate ($LiNbO_3$), which has motivated the development of BTO-based photonic devices. Nowadays the most common modulation mechanism used in silicon devices is the plasma dispersion effect [6]. However, the modulation speed is limited by the carrier lifetime and optical losses are also induced. The Pockels effect is intrinsically lossless and ultra-fast. In this way, high modulation efficiencies and the potential for achieving modulation bandwidths above 40 GHz have been demonstrated by using BTO deposited on top of magnesium oxide (MgO) substrates [7–11]. However, in the last years, the successful growth of high quality BTO films on silicon has opened a new path for providing electro-optic functionalities to the silicon photonic platform [12–16]. The possibility of an integration process compatible with large

Optical Materials EXPRESS

size silicon wafers makes BTO more attractive than other materials such as lithium niobate in which the integration is based on bonding processes [17].

The electro-optical performance of hybrid BTO/Si modulators has been mostly analyzed under static conditions and simulated modulation efficiencies as low as 0.27 V·cm have been reported [18–21]. However, high speed modulation cannot be achieved unless RF electrodes are properly designed. Hence, an accurate measurement of the relative permittivity of the BTO layer is a prerequisite to accomplish such design task.

The BTO permittivity depends on the crystallographic axes of the material. A value of about 56 for the direction parallel to the optical axis and of about 2200 for the direction perpendicular to the optical axis have been taken as a gauge of good quality of clamped, single-domain crystals [5]. However, the permittivity may show a huge variability depending on the fabrication conditions. Low values between 83 and 120 have been reported for films deposited at room temperature by RF sputtering [22]. Conversely, high values up to 6000 have also been measured and correlated with the grain size and microstructural characteristics of the material [3]. The permittivity may also depend on the thickness of the BTO layer and the frequency of the applied electric field. Values between 230 and 1000 have been measured for BTO films with thicknesses ranging from 30 to 580 nm at a low frequency of 1 KHz [23]. At higher frequencies, a decrease of permittivity from 2200 to 500 has been estimated for RF frequencies among 1 and 40 GHz [24].

In this work, the relative permittivity of thin BTO films deposited on silicon-on-insulator (SOI) substrates is first analyzed. A multiline method is proposed to estimate the effective permittivity at wafer level and then electromagnetic simulations are carried out to extract the BTO permittivity. Therefore, the BTO can be characterized in the same growth conditions as the ones used to fabricate the devices. Once the BTO permittivity is obtained, RF electrodes have been designed for high speed modulation in hybrid BTO/Si devices. Finally, the designed electrodes have been fabricated and characterized.

2. BTO fabrication process

BTO layers have been grown on a SOI substrate with a device silicon layer thickness of 100 nm and a buried oxide thickness of 2 μm. A thin (3-4 nm thick) $SrTiO_3$ buffer is required to accommodate the crystallographic and chemical heterogeneity between BTO and Si and ensure single crystallinity and high crystal quality of the BTO layer. Molecular beam epitaxial (MBE) was used to grow the $SrTiO_3$ template, as described in [12] and [25]. Then, two different approaches, MBE and RF sputtering, were employed to grow the BTO layer with a thickness of about 50 nm.

RF-sputtering was used to grow 50 nm-thick BTO film on the $SrTiO_3$/SOI template. A BTO stoichiometric target was sputtered under Ar and O_2 mixing atmosphere and using a RF generator at a substrate temperature of 650°C. After growth, the BTO layer was submitted to rapid thermal annealing to improve its structural quality and ensure good oxidation of the thin layer. On the other hand, using a similar $SrTiO_3$/Si template, a 50 nm thick BTO was grown by MBE using Ba and Ti co-deposited at 600°C under an oxygen partial pressure of about 10-5 Torr. More details can be found in [12].

3. RF characterization of the BTO layer

The relative permittivity of the BTO has been characterized on the same multilayer stack, shown in Fig. 1, used to develop the optimum travelling-wave electrodes for high speed modulation. In this case, the BTO permittivity cannot be measured as in a conventional capacitor by extracting the capacitance between its plates [1]. Therefore, a multi-line method [26, 27] can be used to estimate the effective permittivity of the complete multilayer stack. The proposed method is part of the well-known Thru-Reflect-Line (TRL) algorithm and has the advantage of allowing on-wafer characterization [28, 29].

Optical Materials EXPRESS

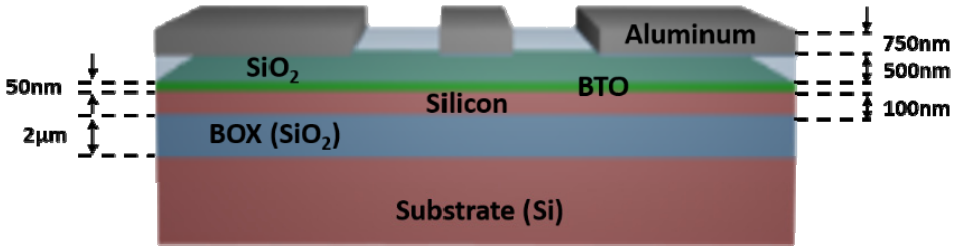

Fig. 1. RF coplanar waveguide structure used to characterize the BTO permittivity.

RF coplanar waveguides (CPW) were fabricated on top a 500 nm-thick SiO_2 layer deposited by PECVD on the BTO/SOI substrate. The CPWs have a gap of 45 µm and a width of 45 µm for the central line. The metal is aluminum with a thickness of 750 nm. Transmission lines with different lengths were used to apply the multiline method. A length of 1 mm was chosen for the thru (reference) line while lengths of 2 mm, 2.5 mm and 3 mm were used for the other lines. The difference in length between the thru and the rest of the lines is acceptable for minimizing the inaccuracy caused by the manual alignment of RF probes on the metal pads. The scattering parameters of the CPW were measured and then used to extract the effective permittivity by applying the multi-line method described below. The BTO relative permittivity was obtained by matching the simulated effective relative permittivity with the one obtained by measurements.

3.1 Characterization of the effective permittivity

The multi-line method allows to obtain the complex propagation constant (γ) and the effective permittivity of the multilayer stack through the following equation [30]:

$$\varepsilon_{eff} = -\left(\frac{\gamma c}{2\pi f}\right)^2 \tag{1}$$

where c is the speed of light and f is the RF frequency. One of the main advantages of this method is that it does not require vector network analyzer (VNA) calibration to measure the scattering parameters (S_{11}, S_{12}, S_{21} and S_{22}). Figure 2 shows the fabricated CPWs with different lengths.

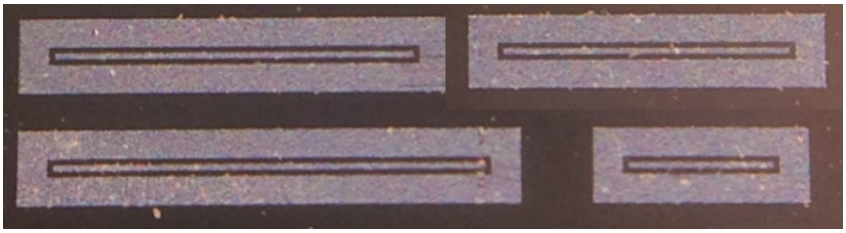

Fig. 2. Fabricated CPWs with lengths between 1 mm and 3 mm.

To apply the method, the scattering parameters matrix are first converted into transmission parameters

$$T = \frac{1}{S_{21}}\begin{pmatrix} -\Delta & S_{11} \\ -S_{22} & 1 \end{pmatrix} \tag{2}$$

with

Optical Materials EXPRESS

$$\Delta = S_{11}S_{22} - S_{12}S_{21} \tag{3}$$

The use of transmission matrices instead of scattering parameters has the advantage of exploiting the cascade multiplying property. Let the transmission matrices of the thru (reference line with shortest length) and of the longer delay lines to be denoted as T_t and T_d respectively. T_1 and T_2 represent the error matrices introduced in each port of the uncalibrated VNA. Thereby, the measured transmission matrices can be expressed as

$$T_t = T_1 T_2 \tag{4}$$

$$T_d = T_1 T_l T_2 \tag{5}$$

where T_l represents the delay line without the error

$$T_l = \begin{pmatrix} e^{-\gamma\Delta l} & 0 \\ 0 & e^{\gamma\Delta l} \end{pmatrix} \tag{6}$$

and Δl represents the length difference between thru and the respective delay line. The following matrix elements can be calculated from the measured matrices by

$$\begin{pmatrix} t_{11} & t_{12} \\ t_{21} & t_{22} \end{pmatrix} = T_d T_t^{-1} \tag{7}$$

such that the propagation constant can be calculated as

$$\gamma = \frac{1}{2\Delta l} \ln\left(\frac{t_{11} + t_{22} \pm \sqrt{(t_{11} - t_{22})^2 + 4t_{12}t_{21}}}{t_{11} + t_{22} \mp \sqrt{(t_{11} - t_{22})^2 + 4t_{12}t_{21}}} \right) \tag{8}$$

where the influence of the error matrices, T_1 and T_2, has been suppressed [28]. The sign assignment in Eq. (8) should be such that $|e^{2\gamma l}|<1$. Finally, the real part of the effective permittivity is obtained from Eq. (1).

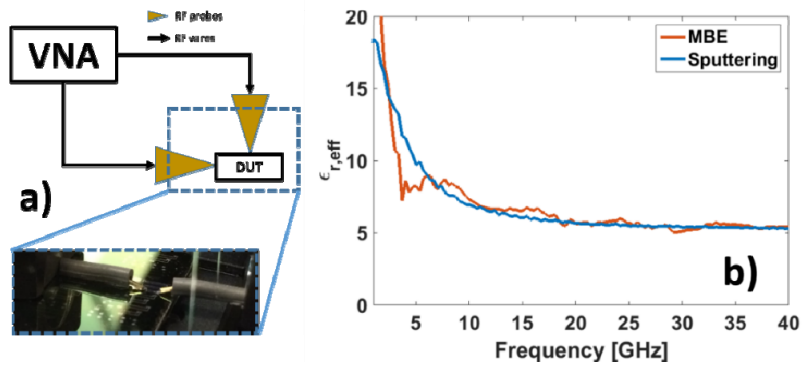

Fig. 3. (a) Schematic of the measurement set-up by using a vector network analyzer (VNA) and photo zoom in the device under test (DUT) area, and (b) measured effective permittivity as a function of the RF frequency for the samples with BTO fabricated by MBE and RF sputtering.

Figure 3(a) shows a schematic of the measurement set-up. Figure 3(b) shows the real part of the effective permittivity as a function of the RF frequency by using the transmission matrix of the 2 mm long delay line in Eq. (5). Similar results are obtained when considering the other delays lines. The effective permittivity is also very similar for the samples with BTO fabricated by MBE or RF sputtering.

Optical Materials EXPRESS

3.2 Estimation of the BTO relative permittivity

Simulations by COMSOL Multiphysics have been carried out to obtain the microwave index of the quasi-TEM mode that propagates in the CPW. Figure 4(a) shows the electric field distribution of the quasi-TEM mode at the frequency of 20 GHz. The microwave index n_m is directly related to the effective permittivity.

$$n_m = \sqrt{\varepsilon_{eff}} \tag{9}$$

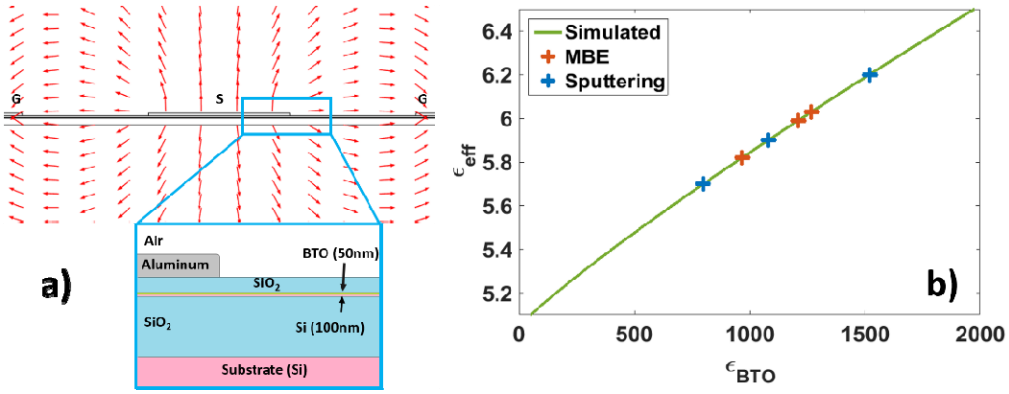

Fig. 4. (a) Simulated electric field distribution of the quasi-TEM mode at the frequency of 20 GHz. The inset shows with more detail the CPW structure, and (b) simulated effective permittivity of the CPW as a function of the BTO relative permittivity and measured values extracted at 20 GHz from the different delay lines fabricated in the samples with BTO grown by MBE and RF sputtering.

The relative permittivity of the BTO layer has been modified in the simulations to match the real part of the effective permittivity with the measured values. Figure 4(b) shows the obtained simulation results for 20 GHz and the measured values extracted from the different delay lines for both BTO fabrication processes. The BTO layer has a relatively small influence on the effective permittivity due to its low thickness. Simulation and experimental values are matched for a BTO permittivity between 800 and 1600. Hence, an average value of 1200 has been chosen to design the optimum electrodes for high speed modulation. The high value obtained for the BTO is in agreement with BTO grown mostly with c-axis ferroelectric domain orientation [5, 24], which was confirmed by X-ray diffraction (XRD) measurements

4. RF electrodes design for modulator

The hybrid BTO/Si optical waveguide depicted in Fig. 5(a) has been proposed for enabling electro-optical modulation with high performance. A layer of amorphous silicon (a-Si) is deposited on top of the BTO/SOI structure and then etched down to form the optical waveguide. The influence of the waveguide parameters on the static electro-optical performance has been previously reported [20]. The electrodes are placed on top of the BTO layer after opening lateral windows in the SiO_2 cladding to enhance the modulation efficiency.

The high value of the BTO relative permittivity (ε_r~1200) will increase the capacitance of the electrodes and thus the impedance will be reduced with respect to materials with lower dielectric constants. A narrow gap between electrodes and the optical waveguide is desirable to improve the modulation efficiency though a too small value will give rise to optical losses due to interaction of the optical mode with the metal electrodes [20]. Coplanar strip-line (CPS) electrodes have been designed to achieve the best modulation performance in a travelling-wave configuration.

Optical Materials EXPRESS

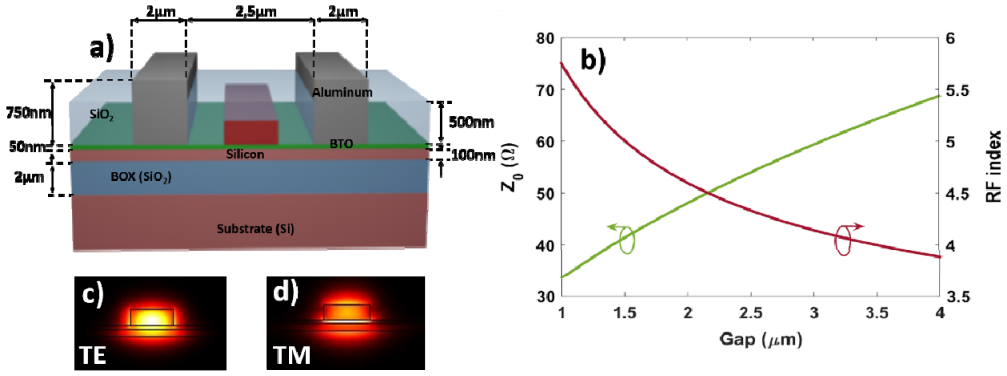

Fig. 5. (a) Hybrid BTO/Si optical waveguide with coplanar strip-line electrodes and (b) simulated impedance of the CPS electrode and microwave index of the RF mode at 20 GHz as a function of the gap and for an electrodes width of 2 µm, (c) optical mode profile for TE and (d) TM polarizations.

The maximum thickness of the metal electrodes allowed by the fabrication process, which is around 750 nm as depicted in Fig. 5(a), has been initially fixed. The gap and width of the CPW electrode have then been designed taking into account their influence on the impedance and microwave index. Both impedance and microwave index decrease when the electrode width increases. However, they change in an opposite way when the gap is varied, as it is shown in Fig. 5(b). The microwave and optical group indices should be matched to maximize the bandwidth. The simulated optical group index of the hybrid BTO/Si optical waveguide is 3.66 for TE polarization (Fig. 5(c)) and 3.85 for TM polarization (Fig. 5(d)). Thereby, the optimum parameters of the CPS electrode have been found for a gap of 2.5 µm and an electrodes width of 2 µm. The resulting impedance and microwave index are 54 Ω and 4.52, respectively, as it can be observed in Fig. 5(b). An impedance close to 50Ω allows achieving maximum voltage transfer and avoids electrical reflections. In addition, the potential bandwidth by assuming negligible microwave propagation losses (α = 0) can be easily estimated by

$$\Delta f = \frac{2c}{\pi L(n_m - n_o)} \tag{10}$$

where c is the speed of light, L is the modulation length and n_m and n_o are the microwave and optical group indices [30]. Bandwidths higher than 40 GHz for modulation lengths up to 5.5 mm would be feasible based on Eq. (10). The designed CPS electrode has been fabricated and characterized. The experimental impedance was extracted from the reflection coefficient of the scattering parameters. Figure 6(a) shows the simulated and experimental impedance as a function of the RF frequency. It can be seen that the influence of the BTO fabrication process on the experimental impedance values is low. Furthermore, there is a rather good agreement between simulation and experimental results.

The microwave propagation losses have also been extracted from the measured scattering parameters. Propagation losses are mainly originated due to conductor and dielectric losses [31]. Conductor losses have a square root dependence with frequency due to the skin effect. Besides, dielectric losses depend on the polarization and ohmic losses of the dielectric materials. At high frequencies, the heating associated with the polarization become the dominant source of losses. Figure 6(b) shows the experimental losses as a function of the RF frequency. Simulations considering conductor losses have also been carried out to compare with experimental results. The difference between experimental and simulation results increases for high RF frequencies. Such higher losses are attributed to dielectric losses of the

Optical Materials EXPRESS

materials but also from additional conductor losses due to surface roughness at the electrodes. However, it is interesting to notice that the sample with BTO fabricated by sputtering has higher losses than the sample with BTO growth by MBE. Therefore, the obtained results also suggest that BTO losses may play an important role and that lower losses are achieved by MBE.

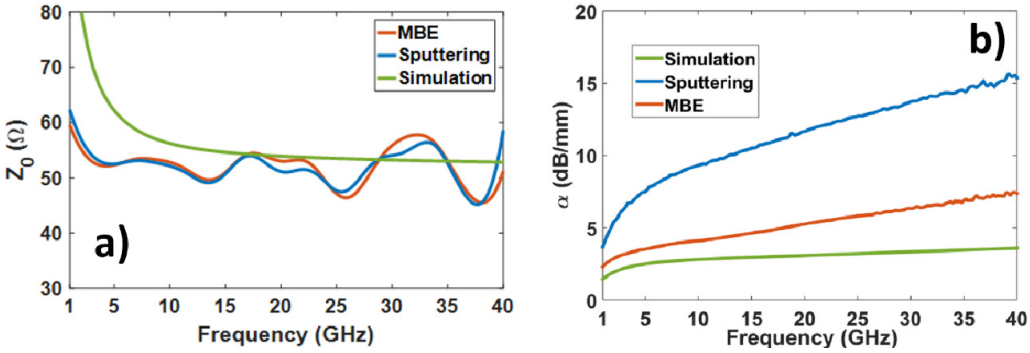

Fig. 6. Simulated and experimental (a) impedance and (b) microwave propagation losses of the designed CPS electrode as a function of the RF frequency. Only conductor losses are included in the simulations.

Furthermore, for a given microwave propagation losses and considering that the CPS electrode is terminated by its impedance, the small signal electro-optical modulation response can be calculated by

$$T_{EO}(f) = e^{-\frac{\alpha L}{2}} \sqrt{\frac{\sinh^2\left(\frac{\alpha L}{2}\right) + \sin^2\left(\frac{2}{\Delta f}\right)}{\left(\frac{\alpha L}{2}\right)^2 + \left(\frac{2}{\Delta f}\right)^2}} \tag{11}$$

where L is the modulation length, α is the loss coefficient, Δf is given by Eq. (10) and f is the RF frequency [32].

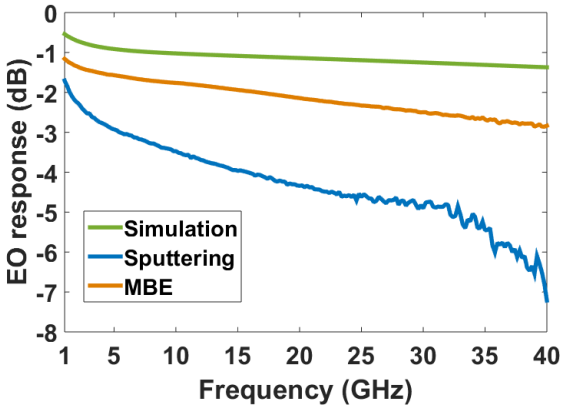

Fig. 7. Simulated electro-optical modulation response for a modulation length of 1.5 mm, TM polarization and taking into account the simulated and measured microwave losses.

Figure 7 shows the simulated frequency response for a modulation length of 1.5 mm, TM polarization and taking into account the simulated and measured microwave losses depicted

Optical Materials EXPRESS

in Fig. 6(b). The electro-optical response is practically the same for TE polarization (n_o = 3.66). Therefore, for both light polarizations, the modulation bandwidth would be drastically reduced to around 5 GHz for the BTO grown by sputtering due to the high losses. However, a modulation bandwidth of 40 GHz would be achieved for the BTO grown by MBE. Furthermore, a half-wave voltage, V_π, of around 5 V for TM polarization and 7.9 V for TE polarization has been obtained by simulation for *c*-axis oriented BTO and the modulation length of 1.5 mm.

5. Conclusions

A multi-line method combined with electromagnetic simulations has been proposed and demonstrated to obtain the relative permittivity of BTO thin films deposited on top of a SOI substrate. In such a way, the permittivity can be obtained at wafer level and at the same process conditions used for fabricating the devices. Similar values around 1200 at high RF frequencies have been obtained for BTO grown by two different techniques: MBE and sputtering. The high permittivity value is associated with the c-axis ferroelectric domain orientation of the BTO layer.

A coplanar strip-line electrode has also been designed and experimentally demonstrated for high speed modulation in a hybrid BTO/Si device. The modulation bandwidth is limited by the microwave propagation losses. Lower losses have been obtained by MBE compared to RF sputtering which suggest that process conditions could be optimized to minimize the dielectric losses of the BTO layer. Nevertheless, modulation bandwidths up to 40 GHz have been demonstrated to be feasible.

Funding

Financial support from European Commission under project FP7-ICT-2013-11-619456 SITOGA, and from TEC2016-76849-C2-2-R and NANOMET Conselleria de Educació, Cultura i Esport -PROMETEOII/2014 034 are acknowledged. Álvaro Rosa also acknowledges the Spanish Ministry of Economy and Competitiveness for funding his grant.